Proceedings of the 21st ICSMGE, Vienna, Austria, 14 – 19 June 2026. Pistrol, Adam & Schweiger (eds.)
Published by: ÖGG, Austrian Society for Geomechanics, Salzburg, Austria, ISBN 978-3-9503898-4-5
https://doi.org/10.53243/ICSMGE2026-1832

A Hardening Soil model with improved small-strain stiffness

Ricardo J. N. Azeiteiro
Seequent, the Bentley Subsurface Company, London, United Kingdom, ricardo.azeiteiro@seequent.com

Ilaria Del Brocco [(1)], Evira Eman [(2)], Ronald B. J. Brinkgreve [(1,2)], Tuan A. Bui [(1)], Sandro Brasile [(1)]
[(1)] *Seequent, the Bentley Subsurface Company, Delft, The Netherlands*
[(2)] *Delft University of Technology, CEG, Geo-engineering, Delft, The Netherlands*

ABSTRACT: The Hardening Soil (HS) model has been widely used for the simulation of geotechnical problems. Its popularity has been sustained by its ability to simulate some of the key features of soil response, such as stress dependency, dilatancy and highly non-linear pre-failure response, associated with its relatively simple and clear calibration process based on standard laboratory and field test results and well-established empirical formulas. To improve its ability to deal with unloading, the model was later extended with a small-strain stiffness formulation, leading to the HS-small model. It has become a natural choice for simulations involving retaining walls, shafts and tunnels. Moreover, given the hysteretic nature of the small-strain stiffness formulation, the HS-small model has also emerged as a suitable choice for the simulation of wave propagation and vibration problems within the small to medium strain range. However, as many other constitutive models based on non-linear hysteretic elasticity (or plasticity), it has been recently found that HS-small can suffer from overshooting issues, which are characterised by an overprediction of stiffness after the occurrence of minor unloading-reloading cycles, due to the reset of the strain history tensor. Besides being often found in dynamic problems (e.g. vibrations induced by pile driving, traffic loading or machine operation), these issues may generally affect all boundary-value problem simulations, where numerical oscillations often produce spurious unloading-reloading perturbances. It is therefore imperative to address them. In this paper, the fundamental ingredients of two novel small-strain stiffness formulations addressing overshooting issues in practical applications are presented. The results of laboratory test simulations, including small unloading-reloading cycles interpreted as perturbances, show that both proposed formulations are able to prevent overshooting issues in HS-small.

KEYWORDS: Hardening Soil model, small strain stiffness, overshooting, constitutive modelling.

1 INTRODUCTION

Since its implementation into PLAXIS, the Hardening Soil with small strain stiffness (in short, HS-small) model has been widely adopted for the simulation of many geotechnical problems, with particular emphasis on those involving excavations. Although relying on well-established concepts, its small strain component may exhibit overshooting issues (i.e. overpredict the stiffness of the material) in situations where small unloading-reloading cycles (often unexpected from modelling sequence) trigger the reset of the accumulated strain history. In this paper, after a comprehensive explanation of the causes of the overshooting issues in the HS-small model, two novel formulations specifically developed to tackle these issues are presented. Both formulations consider a robust, but computationally economical extension of the strain history tensor (i.e. loading memory) to be able to correct the elastic shear stiffness of the material upon closing of each small unloading-reloading cycle. Their ability is shown in the context of element laboratory test simulations.

2 BACKGROUND TO THE HARDENING SOIL WITH SMALL STRAIN STIFFNESS MODEL

2.1 *Original formulation of the Hardening Soil model*

The Hardening Soil (HS) model was originally proposed by Schanz *et al.* (1999). It is formulated within the elasto-plasticity theory and uses the following two isotropic hardening yield surfaces:

- a deviatoric strain-hardening Duncan & Chang (1970)'s hyperbolic type yield surface, with a non-associated Rowe (1962)'s type flow rule;
- an associated volumetric strain-hardening (i.e. cap-type) yield surface, which introduces plasticity for isotropic- and oedometer-type of stress paths.

In addition, the HS model uses the well-known Mohr-Coulomb failure criterion to define the ultimate shear strength of the material, as well as a Rankine-type tension cut-off criterion (optional).

Another relevant feature of the constitutive model consists of its stress dependency. Specifically, the deviatoric strain-hardening yield surface makes use of a secant stiffness modulus, which depends on a function, f_σ, of the minor principal effective stress, σ'_3, as given by Equation (1).

$$f_\sigma = \left(\frac{\sigma'_3 + c' \cot \varphi'}{p'_{ref} + c' \cot \varphi'} \right)^m \tag{1}$$

where p'_{ref} is a reference pressure typically taken as the atmospheric pressure, c' is the apparent cohesion, ϕ' is the friction angle and m is the non-linearity coefficient, all of them being (user-defined) model parameters.

Similarly, the hardening law of the cap yield surface is calibrated such that the tangent stiffness obtained in oedometer-type loading can be described as a function of σ'_3 and of the coefficient of the earth pressure at rest in normal consolidation, K_0^{NC}. Finally, the isotropic elastic component of the HS model also incorporates the σ'_3-dependency law used by the plastic component (i.e. it considers hypoelasticity) and assumes a constant Poisson's ratio. For further details, refer to Schanz *et al.* (1999) or to PLAXIS (2025).

2.2 *The original small strain stiffness extension of the Hardening Soil model*

To describe the non-linear response of soil within the small strain range, the HS model was later extended by Benz (2007), leading to the Hardening Soil model with small strain stiffness, henceforth termed simply as HS-small model. Specifically, the stress-dependent elastic component of the HS model was replaced by a stress- and strain-dependent hysteretic (i.e. using a set of unloading-reloading rules) elastic formulation of Hardin & Drnevich (1972)'s hyperbolic type, whose backbone curve can be described by Equation (2).

$$\tau = G_0 \frac{1}{1 + a\dfrac{\gamma_{hist}}{\gamma_{0.7}}}\,\gamma_{hist} \qquad (2)$$

where $a = 0.385$ is a model constant, while $G_0^{ref} = f_\sigma\, G_0$ and $\gamma_{0.7}$ are model parameters representing, respectively, the maximum elastic shear strain stiffness at the reference pressure (typically defined for shear strain levels smaller than 1×10^{-6} m/m) and the shear strain level at which the secant elastic shear stiffness is reduced (when using $a = 0.385$) to about $1/(1 + 0.385) \approx 0.722$ of its maximum value (i.e. 0.722 G_0). Moreover, the quantity γ_{hist} defines the current shear strain measure, which is obtained by projecting the strain history tensor, $\boldsymbol{H}$, onto the current deviatoric strain increment direction, $\delta\boldsymbol{e}/\|\delta\boldsymbol{e}\|$ (with $\|\boldsymbol{a}\| = \sqrt{\boldsymbol{a}:\boldsymbol{a}}$ being the Euclidean norm), as defined by Equation (3).

$$\gamma_{hist} = \sqrt{3}\,\frac{\|\boldsymbol{H}:\delta\boldsymbol{e}\|}{\|\delta\boldsymbol{e}\|} \qquad (3)$$

Note that $\boldsymbol{H}$ is a elastic state variable, being updated at every step by summing the current value of $d\boldsymbol{e}$ to the value of the $\boldsymbol{H}$ at the start of the step. Moreover, $\boldsymbol{H}$ is affected by the detection of strain reversals (SRs). According to the methodology proposed by Benz (2007), a SR occurs when any of the diagonal components of $d\boldsymbol{e}$, rotated to its eigen system (i.e. any of its eigenvalues, λ_i, with i = 1 to 3), has an opposite sign to that of $\boldsymbol{H}$ also rotated to the eigen system of $d\boldsymbol{e}$, $\overline{H}_i$, (i.e. $\overline{H}_i\,\lambda_i < 0$).

Once a SR is flagged, the corresponding diagonal component of the rotated $\boldsymbol{H}$ is set to zero by using a transformation matrix, as detailed in Benz (2007), after which $\boldsymbol{H}$ is rotated back to the cartesian system.

Additionally, in proportional strain loading (e.g. triaxial compression loading path) the directions of $\boldsymbol{H}$ and $d\boldsymbol{e}$ are colinear, in which case the following conditions are observed: (i) if there are no SRs (i.e. monotonic loading), then $\gamma_{hist} = \sqrt{3/2}\,\|\Delta\boldsymbol{e}\|$, where $\Delta\boldsymbol{e}$ is the accumulation of deviatoric strain; (ii) whenever a SR occurs, γ_{hist} becomes momentarily zero and, consequently, the maximum shear strain stiffness, G_0, is retrieved.

Four additional aspects of the HS-small model should be highlighted:

1. the current value of the secant elastic shear stiffness modulus at a reference pressure, G_{act}^{ref}, is stored in the state variable vector not only for output purposes, but also to ensure that the current shear stiffness is known even if no deviatoric strain increment is applied in a given step (i.e. when $\|\delta\boldsymbol{e}\| \sim 0$, in which case Equation (3) would become undefined);
2. the minimum ever reached value of the ratio of the secant elastic shear stiffness modulus when using a unitary scaling factor at a reference pressure to the unloading-reloading modulus at a reference pressure, $G_{act,i}^{ref}/G_{ur}^{ref}$, is also stored in the state variable vector and used to scale the plastic hardening laws – refer to Benz (2007) for further details;
3. according to the second basic Masing (1926)'s rule, once a SR occurs, the stress-strain response follows the backbone function translated to the SR point and scaled by a given factor N, as defined by Equation (4) (where the subscript "SR" means updated at the last SR point); note that, in the majority of the constitutive models based on this framework (refer e.g. to Taborda, 2011), N is initialised as 1 and changed to 2 once a first SR is detected; however, in HS-small, a different choice is made: N = 2 is used throughout loading; in effect, as explained by Benz (2007), given that the deviatoric strain-hardening yield surface is active since the start of loading, the 'primary' response (i.e. before the occurrence of any SR) is necessarily softer than that in unloading or reloading, removing the need for changing the value of the scaling factor N.

$$\tau = \tau_{SR} + \frac{G_0}{1 + \dfrac{a\,(\gamma_{hist} - \gamma_{hist,SR})}{N\,\gamma_{0.7}}}\,(\gamma_{hist} - \gamma_{hist,SR}) \qquad (4)$$

4. similar to the HS model, the elastic component of the HS-small model also makes use of a constant Poisson's ratio; the elastic components of both models are isotropic;
5. besides all aforementioned differences in their elastic components, the HS-small model employs a different plastic flow rule from that of the HS model; refer to Benz (2007) or to PLAXIS (2025) for further details.

3 UNDERSTANDING THE OVERSHOOTING ISSUE

Whenever a strain reversal (SR) is detected, the strain history tensor, $\boldsymbol{H}$, of the HS-small model is (at least partially) reset to zero. Moreover, as dictated by the second basic Masing rule, the backbone curve is translated to the SR point, with the same function being used to describe the strain-dependent shear elastic stiffness onwards. A problem may occur if a second SR occurs shortly after and the stress point is brought back to the point before the first SR. In such case, it is often observed that the elastic shear stiffness, G, at the end of the unloading (UL) – reloading (RL) cycle is higher than that obtained prior to the cycle, a problem known in the literature as 'overshooting'. This issue is illustrated in Figure 1, where it can be seen that the values of G at point 1 are different before and after the small UL-RL cycle (black solid curve), compared to what would be obtained in monotonic loading (grey dotted curve). As it will be clearer later, the issue is related to the fact that the previous memory of loading relies solely on the state at last SR.

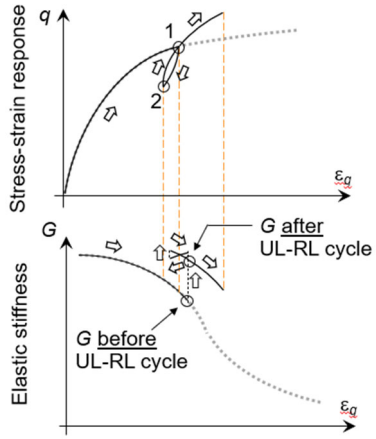

Figure 1. Schematic illustration of the overshooting issue.

The impact of the overshooting on the overall response depends on many factors, including: (1) strain level (in comparison with the cut-off strain level) at which the UL-RL cycle is initiated; (2) the previous loading history (which affects the values of the state variables, including $G_{act,i}^{ref}/G_{ur}^{ref}$, which, as mentioned before, is used to scale the plastic hardening modulus); (3) whether the elasto-plastic response is resumed after the UL-RL cycle or not, which naturally affects the overall stress-strain response obtained after the UL-RL cycle (i.e. overshooting may be overshadowed by the overall impact of the plastic component on the modelled response) (4) cyclic strain amplitude of the UL-RL cycle itself, with the higher impact

being observed for smaller UL-RL cycles; (5) stress path, etc. The dependency on all these factors (with particular emphasis on the previous loading history) makes it very challenging to address the overshooting issue, particularly at a reasonable computational cost (including the use of a reasonable number of state variables). Moreover, the fact that, in many practical applications, this issue is often overshadowed by the impact of the plastic component on the modelled response (i.e. the stiffer elastic response arising from overshooting is masked by the dominant plastic response) has likely contributed to the fact that this issue has rarely been addressed. In effect, although a set of extended Masing rules has been proposed a long time ago, they have rarely been considered in constitutive modelling (Taborda, 2011). Conversely, simpler solutions, such as a variable scaling factor (Pyke, 1979), have been proposed to tackle this issue, particularly when dealing with purely elastic (or paraelastic) models (even if coupled with a failure criterion).

4 IMPROVED SMALL STRAIN STIFFNESS FORMULATIONS

4.1 *General aspects*

Given the relevance of the small strain component of the HS-small for the prediction of some boundary value problems (BVPs), particularly those involving unloading (Benz, 2007), and the potential occurrence of overshooting issues in those types of problems, either as a result of the load/boundary conditions or simply due to the numerical nature of the method (e.g. stress redistribution), a research study was undertaken with the main objective of developing a formulation able to minimise overshooting while keeping the computational cost of the model integration at an acceptable level. A choice was made to retain the main ingredients of the HS-small model, such as: (a) the hypoelastic nature arising from the use of the stress-dependency function given by Equation (1); (b) the Hardin & Drnevich (1972)'s hyperbolic type, as described by Equation (2); and (c) the conformity with the basic Masing rules. In addition, a correction of the elastic stiffness at the moment at which 'virgin' loading is reset (i.e. the material returns to a state never experienced before, according to a given previous loading memory) was preferred over a gradual decrease in stiffness from the start of reloading. Finally, since the main scope of application of the HS-small model concerns static analysis, it was considered enough to retain in memory what happens in the most recent loading cycle, but not in the cycles prior to that one, which would naturally have a higher computational cost (and, therefore, loss of performance).

4.2 *A continuous brick (CB) formulation*

4.2.1 *Basic framework*

The starting point of this formulation was the 'discontinuous' brick formulation originally proposed by Simpson *et al.* (1979) and applied by Cudny and Truty (2020) to their version of the HS-small model. It uses the concept of nested circular surfaces in the deviatoric strain space, which move with the current deviatoric strain. Each of these surfaces is characterised by a given radius (often called 'string length' within this framework) and associated with a given 'brick' point, which is allowed to be inside its corresponding surface or on it (in which case, the brick is active), but never outside of it (which means that eventually the brick points will move with the current deviatoric strain point upon becoming active). Moreover, each of the surface radii defines a point in the tangent elastic shear stiffness, G, – shear strain measure, γ_{hist}, curve (note that $\gamma_{hist} = \sqrt{3/2}\sqrt{\Delta\boldsymbol{e}:\Delta\boldsymbol{e}}$, where $\Delta\boldsymbol{e}$ is the deviatoric strain accumulation, is used in this framework). As such, once a given brick becomes active, its corresponding G value is employed in the simulation (resulting in a stepwise G reduction with increasing strain level). These concepts are illustrated in Figure 2. It can be seen that, at the start of loading, all bricks (represented as points coloured other than grey) and the current deviatoric strain (represented as a grey point) are located at the origin, with G having its maximum value (Figure 2a). Once (deviatoric) loading starts, the deviatoric strain point moves in the space, with all surfaces moving along, while keeping their centres at the deviatoric strain point. At some point, the surface corresponding to brick 1 (i.e. with shortest radius) starts containing its corresponding brick point, meaning that G is stepwise decreased by a given amount (Figure 2b). Supposing that straining continues along the same direction, eventually all bricks become active, therefore moving in the space (Figure 2c). Interestingly, once a strain reversal (SR) occurs and the deviatoric strain moves in the opposite direction (i.e. unloading (UL) is triggered), the surfaces no longer contain the bricks points and, consequently, all of them become inactive (i.e. still in the space) and maximum G is recovered , as illustrated in Figure 2d. Supposing that another SR would happen slightly afterwards triggering reloading (RL) the exact same configuration shown in Figure 2c would be recovered once the deviatoric strain point would move back the same distance undergone in UL (i.e. once the UL-RL cycle would be closed), and G prior to that UL-RL cycle would be reset, as intended.

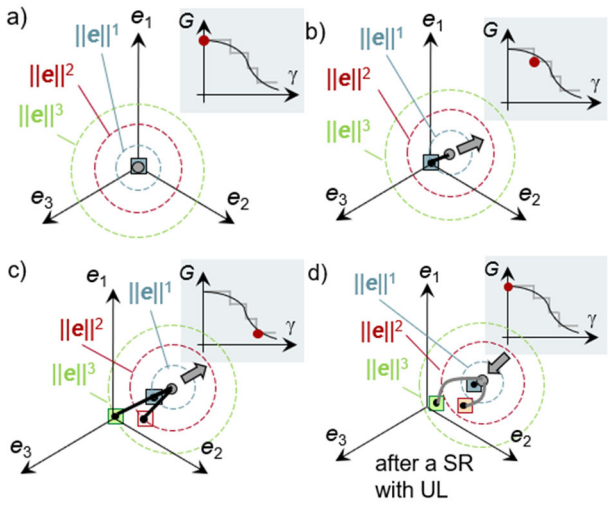

Figure 2. The 'discontinuous' brick concept in the deviatoric strain space, as originally proposed by Simpson *et al.* (1979).

Although attractive, this formulation has the following limitations: (1) a discontinuous (i.e. stepwise) reduction of stiffness, which does not represent accurately soil's response; (2) a high cost in terms of state variables, given that each brick is represented by a deviatoric strain point (with 6 components) in the 3D space; as such, if a total of 10 bricks would be used, as suggested by Cudny and Truty (2020), then it would imply a total of 60 components stored in memory just for the brick positions.

To overcome these limitations, a novel formulation, called 'continuous brick' (CB), was developed by retaining the main ingredients of the 'discontinuous brick' formulation. Those ingredients (as well as the operations required for the integration of the discontinuous formulation, such as strategy to detect strain reversals, evolution laws for the bricks, etc) are not detailed here, since they can be found in Simpson *et al.* (1979) and Cudny and Truty (2020).

4.2.2 *Continuous elastic shear stiffness reduction with deviatoric strain level*

In the CB formulation, only two bricks are used, specifically: one brick characterised by a very small string length, $s_{b,brick1}$, which will likely follow the current deviatoric strain point throughout loading; and the 'cut-off brick' having a 'string length' corresponding to the cut-off shear strain measure, $\gamma_{cut\text{-}off}$ (Equation (5)), which, upon activation, defines the onset of the minimum tangent elastic shear stiffness (corresponding to the unloading-reloading tangent elastic shear modulus, G_{ur}), as illustrated in Figure 3.

$$\gamma_{cut-off} = \frac{N}{a}\left(\sqrt{\frac{G_0^{ref}}{G_{ur}^{ref}}} - 1\right)\gamma_{0.7} \tag{5}$$

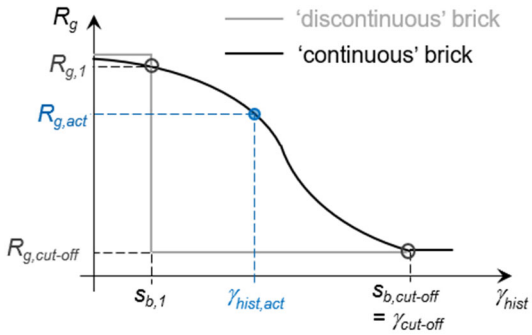

Figure 3. Continuous, rather than stepwise, elastic shear stiffness reduction factor as a function of the shear strain measure.

Moreover, during the integration process, the following information is known:

- which brick is currently active (if any) and which one will be activated next (if any); moreover, since the string length of each brick, s_b, as well as the hyperbolic equation and its parameters are known beforehand, the interval in which the current/actual shear strain measure, γ_{hist}, is located and the corresponding elastic tangent shear stiffness modulus reduction factor, $R_{g,act} = G_{act}^{ref}/G_0^{ref}$, are also known – see Figure 3, where it is assumed that brick 1 is the only brick currently active;
- the shear strain measure accumulation since the activation of a given brick, $\Delta\gamma^*$ (note that the superscript "*" is used to distinguish between the accumulation since the activation of a brick and the accumulation since the last SR); this quantity is updated at every step by adding the change in shear strain measure during the current step, $\delta\gamma^* = \sqrt{3/2}\,\|\delta \boldsymbol{e}\|$, while being reset to zero once a new brick is activated;
- the shear strain measure required to activate the next brick, $\Delta\gamma_{actv}^*$, as described by Equation (6);

$$\Delta\gamma_{actv}^* = \Delta\gamma_0^* + \left[\left(\frac{s_{b,next}}{\|\Delta \boldsymbol{e}^*\|} + \sqrt{\frac{3}{2}}\right)\Delta \boldsymbol{e}^*\right] : \boldsymbol{n} \tag{6}$$

$$with \quad \Delta \boldsymbol{e}^* = \boldsymbol{e_{b,next}} - \boldsymbol{e_0}$$

which depends on the position of the brick to be activated next, $\boldsymbol{e_{b,next}}$, as well as on the position of the deviatoric strain at the start of the step, $\boldsymbol{e_0}$, and its direction during the current step, $\boldsymbol{n} = \delta \boldsymbol{e}/\|\delta \boldsymbol{e}\|$; note that, to account for the fact $\boldsymbol{n}$ may change after the activation of the brick, this quantity is updated in every step, with $\Delta\gamma_0^*$ corresponding to the value of $\Delta\gamma^*$ at the start of the step.

Given the available information, the actual shear strain measure, $\gamma_{hist,act}$, can be computed by using Equation (7).

$$\gamma_{hist,act} = \gamma_{b,last} + \frac{\Delta\gamma^*}{\Delta\gamma_{actv}^*}\left(\gamma_{b,next} - \gamma_{b,last}\right) \tag{7}$$

4.2.3 *Adding the previously accumulated shear strain measure upon reloading*

In the original discontinuous version, the existence of many bricks allows the formulation to predict a sudden drop of elastic shear stiffness once a UL-RL cycle is closed (i.e. to recover the elastic shear stiffness prior to the UL-RL cycle) as a result of the activation of multiple bricks at once. In the continuous version, the fact that only two bricks are used means that the formulation has no longer this ability, except when the elastic stiffness drops to its minimum by activating both brick 1 and cut-off brick. To compensate for this shortcoming, an additional mechanism is introduced, consisting of:

1. storing in memory the shear strain measure accumulation since the activation of a brick up to the last SR with UL, $\Delta\gamma_{SR,UL}^*$;
2. once a SR with UL is detected, the shear strain measure accumulation since the activation of the (last) brick up to that moment, $\Delta\gamma_{SR,UL}^*$, is stored in memory; moreover, the shear strain accumulation from the last SR with UL to the last SR with RL, $\Delta\gamma_{SR,UL-SR,RL}$, is reset to zero;
3. once a SR with RL is detected, the value of $\Delta\gamma_{SR,UL-SR,RL}$ is updated to the value of $\Delta\gamma$ accumulated since the last SR with UL;
4. once brick 1 is activated in RL, the accumulated value of $\Delta\gamma$ since the last SR with RL is compared against the value of $\Delta\gamma_{SR,UL-SR,RL}$; if the former is greater or equal to the latter, then $\Delta\gamma_{SR,UL}^*$ is added to both $\Delta\gamma^*$ and $\Delta\gamma_{actv}^*$, resulting in a 'jump' in the $R_g - \gamma_{hist}$ curve from the point $(s_{b,1},\ R_{g,b1})$ to $(s_{b,1} + \Delta\gamma_{SR,UL}^*,\ R_g = f\{s_{b,1} + \Delta\gamma_{SR,UL}^*\})$, which corresponds to *the state* prior to the UL-RL cycle.

4.3 *A memory surface (MS)-enhanced formulation*

4.3.1 *Main ingredients*

The concept of a 'recent stress history' surface was originally employed by Stallebrass & Taylor (1997) to introduce the effect of the recent stress path on the stiffness and dilatancy of overconsolidated clay. More recently, a similar 'memory surface' (MS) concept has been employed within the framework of bounding surface plasticity to model the effect of fabric changes relevant to the ratcheting response of sand (e.g. Corti *et al.*, 2016; Liu *et al.*, 2019). Within this class of models, Li and Liu (2020) introduced the concept of a 'maximum pre-stress surface' to minimise overshooting issues. In the current study, this concept is extended by using an isotropically and kinematically evolving surface – here called 'memory surface' (MS) – which bounds the recent cyclic deviatoric loading history. Once attempted to be crossed by the current deviatoric state path, it introduces a correction to the elastic shear stiffness of soil, aiming at preventing or, at least, minimising overshooting.

The evolution law of the MS is schematically illustrated in Figure 4. Initially, the MS expands isotropically with the deviatoric strain point (which is assumed, for simplicity of the presentation, to be null at the start of loading – Figure 4a). However, once a SR with UL occurs, the evolution of the MS is paused, with the deviatoric strain point moving inside (Figure 4b). The evolution of the MS is suddenly restarted once a SR with RL is detected (Figure 4c). Specifically, in this formulation, the MS is relocated to the point where the SR took place, while being resized such that the radius is given by the distance between the two SRs. From this point onwards, the evolution of the MS is once again paused until the moment the deviatoric strain point attempts to cross it – Point 4 in Figure 4d.

At that moment, the MS finally impacts the modelled response by triggering a reset of the strain history tensor, $\boldsymbol{H}$, of the small strain component to its value prior to the UL-RL cycle. Consequently, the elastic shear stiffness prior to the UL-RL cycle is retrieved, as intended. From the moment that the deviatoric strain point lies on the MS, it resumes its isotropic evolution until a new reversal eventually happens. It should be noted that, if point 4 does not coincide with point 2 (which is the case of the figure), then there is an approximation inherent to the reset of the strain history tensor. Although a more sophisticated approach could have been devised (such as modifying $\boldsymbol{H}$ by adding the corresponding $\Delta\boldsymbol{e}$), this approximation is believed to be good enough, particularly given the fact that the impact of this MS on the modelled response is particularly relevant for small UL-RL cycles.

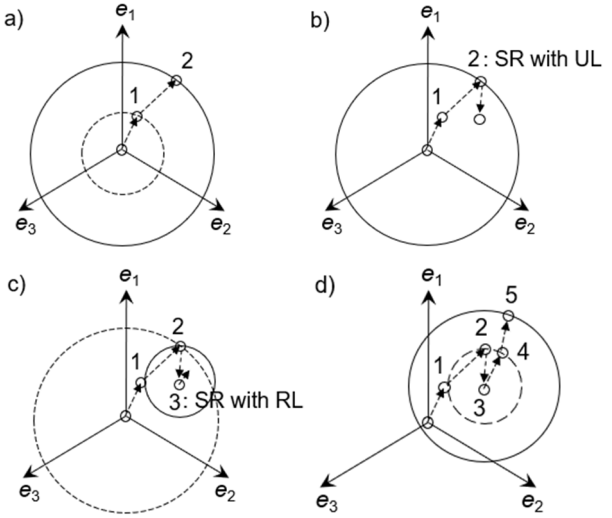

Figure 4. The evolution of the MS in the deviatoric strain space.

Note that, although not presented here, these concepts have been also employed in the deviatoric stress space with equally satisfying results being obtained for element laboratory test simulations.

4.3.2 *Equation of the surface and its state variables*

The MS is defined by Equation (8).

$$F = \|\boldsymbol{e} - \boldsymbol{\alpha}\| - m \tag{8}$$

where $\boldsymbol{e}$ represents the current deviatoric strain, while $\boldsymbol{\alpha}$ and m are the (elastic) state variables required by the MS formulation. More specifically, $\boldsymbol{\alpha}$ is the back deviatoric strain – a tensorial quantity that defines the centre of the surface in the deviatoric strain space – while m is the scalar quantity that defines the opening (i.e. radius) of the surface.

Besides $\boldsymbol{\alpha}$ and m, this formulation requires keeping track of the deviatoric strain at the last SR with UL, $\boldsymbol{e}_{\boldsymbol{SR,UL}}$, which is needed to resize the surface once a SR with RL is detected (Figure 4c), as well as of the strain history tensor at the last SR with UL, $\boldsymbol{H}_{\boldsymbol{SR,UL}}$, which is used for the reset of $\boldsymbol{H}$ upon closing the UL-RL cycle.

4.4 *Similarities and differences between the two newly proposed formulations*

In both CB and MS-enhanced formulations, some state-related quantities are stored at the last SR with UL and used to increase the value of the shear strain measure, γ_{hist}, accumulation upon closing of the UL-RL cycle, which results in a drop in the elastic shear stiffness modulus, G. Note, however, that, while the CB formulation makes use of mostly scalar quantities, the MS-enhanced formulation uses preferentially tensorial quantities. Although being computationally more expensive, it is acknowledged that the use of tensorial quantities may work better in some situations, such as in the presence of spurious strain increments, which may falsify the total length of the strain path (refer to Taborda (2011) for further details).

A more substantial difference resides in the changes to the original small strain formulation. While the MS-enhanced formulation preserves the existing small strain formulation, as proposed by Benz (2007), simply coupling it with the MS concepts, the CB formulation completely reformulates the original small strain formulation (while retaining its main ingredients, such as: hyperbolic form, stress-dependency, etc.). Among the changes introduced by the CB formulation, the following ones are highlighted:

- different SR detection strategy; specifically, in the CB, a SR is considered to have occurred if any of the bricks previously active becomes inactive; since the bricks are represented by points in the deviatoric strain space and nested surfaces, this means that a norm-only-dependent criterion is used, in contrast to the one used in the original small strain formulation, where a check is made along each eigen direction of the deviatoric strain increment tensor (refer to Section 2.2);
- different scaling factor, N; specifically, $N = 1$ (rather than 2) is employed in the CB according to Equation (4); there are two reasons for this choice: (1) the brick framework inherently scales the elastic response in UL and RL in relation to that in 'primary' loading by depending on the distances required to activate the bricks; (2) the use of $N = 1$ is required to compute $G_{act,i}^{ref}/G_{ur}^{ref}$ (to keep compatibility with the existing HS-small plastic hardening law).

Finally, it is important to highlight that, although the MS framework already existed, its application to an elastic component of a model with an extended evolution law is originally proposed in this paper. Similarly, the brick model proposed herein is novel, given its continuous (rather than discontinuous) nature and the use of only two bricks complemented with some scalar-type descriptors of the previous deviatoric strain loading history.

5 ELEMENT LABORATORY TEST SIMULATIONS

A series of single stress point simulations are performed using the PLAXIS SoilTest facility to illustrate the performance of the proposed formulations to correct overshooting. Specifically, for each formulation– original, continuous brick (CB) and memory surface (MS)-enhanced – the following two sets of stress-controlled drained simulations are performed:

1. the 'reference' simulation, consisting of a triaxial extension (TE) shearing phase up to $q = -20\ kPa$ followed by a triaxial compression (TC) shearing phase up to $q = 35\ kPa$ (note that a negative sign for q is used to distinguish TE from TC);
2. the 'small UL-RL cycle' simulation: a loading path identical to that applied in the previous simulation, apart from the fact that, in TC, after every increment of $\Delta q = 5\ kPa$, a small UL-RL cycle with magnitude of $\Delta q = \pm 1\ kPa$ is applied.

In both sets of simulations, the sample is overconsolidated (OCR = 10) and subjected to an initial isotropic effective stress state of 50 kPa. The following model parameters (Amorosi *et al.*, 2016) are used (with default values being assigned to the HS-small model parameters not explicitly mentioned below):
$E_{50}^{ref} = 20\ MPa$; $E_{oed}^{ref} = 20\ MPa$; $E_{ur}^{ref} = 60\ MPa$; $\nu_{ur} = 0.3$; $m = 0.5$; $p_{ref} = 100\ kPa$
$G_0^{ref} = 90\ MPa$; $\gamma_{0.7} = 1.1 \times 10^{-4}\ m/m$
$c'_{ref} = 1\ kPa$; $\phi' = 30°$; $\psi = 0°$

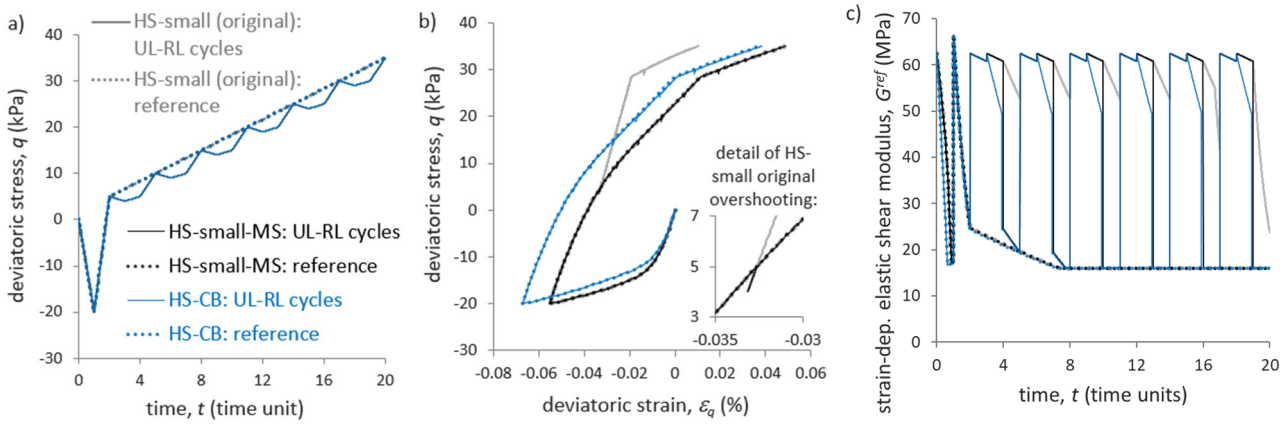

Figure 5. Drained triaxial simulations aiming at assessing overshooting: (a) applied deviatoric stress as a function of time (note that the model is time independent, with time being only used to denote stepping); (b) stress-strain response and (c) evolution of the elastic shear stiffness modulus with time.

The obtained results are compared in Figure 5. It is apparent that, when using the original HS-small model, the response obtained in the 'small UL-RL cycle' simulation departs from that obtained in the 'reference' simulation as soon as the first UL-RL cycle is applied (see figure detail). Conversely, when using both HS-small-MS and HS-CB (i.e. with both improved) versions, the results of the simulations with and without small UL-RL cycles practically overlap (i.e. are overshooting free), as intended. Note, however, that due to the differences in terms of scaling factors explained in Section 4.4, the response obtained when using HS-CB is initially softer (i.e. in TE, before the first strain reversal happens) than that obtained when using HS-small and HS-small-MS, introducing some

Although a sensitivity analysis is not included here for brevity of the presentation, it should be highlighted that the above conclusions remain valid regardless of the chosen model parameters and initial conditions (e.g. OCR value). Moreover, the results of recent simulations of a boundary-value problem (BVP) consisting of a supported excavation with dewatering have suggested that both formulations are nearly-equally effective in minimising overshooting in practical applications, while showing good numerical stability (Eman, 2025). As perceived so far, the preference of the HS-small-MS model over the HS-CB model arises only from its ability to preserve the existing small strain formulation (refer to Section 4.4).

6 CONCLUSIONS

Two novel formulations are proposed to tackle overshooting issues in the HS-small model. One of the formulations – termed "memory surface (MS)-enhanced" – ensures full compatibility with the existing small strain component of the original model and, therefore, preserves the response obtained by the original HS-small model in all situations, with the obvious exclusion of overshooting-affected situations (typically as a result of small UL-RL cycles). The other formulation – termed as "continuous" brick (CB) – implies some alterations to the original formulation (such as the use of a different scaling factor) to comply with the fundamentals of the framework upon which it was developed. Nevertheless, both formulations appear to show great ability to deal with overshooting issues arising from the occurrence of small UL-RL cycles.

Further testing of both formulations is still on-going, particularly in the context of boundary-value problem (BVP) simulations. Besides the evaluation of the ability of both formulations to tackle overshooting, the on-going testing aims at understanding which type of BVPs are more likely affected by this type of issues.

7 REFERENCES

Benz, T. 2007. *Small-Strain Stiffness of Soils and its Numerical Consequences*. PhD thesis. The institute of Geotechnics of the University of Stuttgart, Stuttgart.

Corti, R., Diambra, A., Muir Wood, D., Escribano, D. E. and Nash, D. F. 2016. Memory surface hardening model for granular soils under repeated loading conditions. *Journal of Engineering Mechanics, ASCE*, 142(12), article 04016102-1.

Cudny, M. and Truty, A. 2020. Refinement of the Hardening Soil model within the small strain range. *Acta Geotechnica*, 15, 2031–2051.

Duncan, J.M. and Chang, C.Y. 1970. Nonlinear analysis of stress and strain in soil. *Journal of the Soil Mechanics and Foundations Division, ASCE*, 96, 1629–1653.

Eman, E. 2025. *Verification of two numerical implementations of small-strain stiffness within the HSsmall model*. MSc thesis. Delft University of Technology, the Netherlands.

Hardin, B.O. and Drnevich, V.P. 1972. Shear modulus and damping in soils: design equations and curves. *Journal of the Soil Mechanics and Foundations Division, ASCE*, 98 (SM7), 667–692.

Liu, H.Y., Abell, J.A., Diambra, A., Pisano, F. 2019. Modelling the cyclic ratcheting of sands through memory-enhanced bounding surface plasticity. *Géotechnique* 69(9), 783–800.

Li, Z. and Liu, H. 2020. An isotropic-kinematic hardening model for cyclic shakedown and ratcheting of sand. *Soil Dynamics and Earthquake Engineering*, 138, 1–17.

Masing, V.G. 1926. Eigenspannungen und verfestigung beim messing. *Proceedings of the 2nd International Congress for Applied Mechanics*. Zurich, Switzerland, 12–17 September 1926.

PLAXIS 2025. *PLAXIS 3D material model manual*. PLAXIS 3D 2024.3. Seequent, the Bentley Subsurface Company.

Pyke, R. 1979. Non-linear soil models for irregular cyclic loadings. *Journal of the Geotechnical Engineering Division, ASCE*, 105 (6), 715-726.

Rowe, P.W. 1962. The stress-dilatancy relation for static equilibrium of an assembly of particles in contact. *Proceedings of the Royal Society A: Mathematical, Physical and Engineering Sciences*, 269, 500–527.

Schanz, T., Vermeer, P.A. and Bonnier, P.G. 1999. The hardening soil model: formulation and verification. In: Brinkgreve, R. (ed.). *Beyond 2000 in Computational Geotechnics*. Rotterdam, the Netherlands, CRC Press, 281–296.

Simpson B., O'Riordan N.J. and Croft D.D. 1979. A computer model for the analysis of ground movements in London clay. *Géotechnique* 29(2),149–175.

Stallebrass, S. & Taylor, R. 1997. The development and evaluation of a constitutive model for the prediction of ground movements in overconsolidated clay. *Géotechnique* 47, 235–253.

Taborda, D.M.G. 2011. *Development of constitutive models for application in soils dynamics*. PhD thesis. Imperial College London, United Kingdom.